Excited-State Hydrogen-Atom Transfer along Solvent Wires: Water Molecules Stop the Transfer

Christian Tanner, Markus Thut, Andreas Steinlin, Carine Manca,† and Samuel Leutwyler*

Departement für Chemie und Biochemie, Universität Bern, Freiestrasse 3, CH-3012 Bern, Switzerland

Received: October 26, 2005; In Final Form: November 28, 2005

Excited-state hydrogen-atom transfer (ESHAT) along a hydrogen-bonded solvent wire occurs for the supersonically cooled $n = 3$ ammonia-wire cluster attached to the scaffold molecule 7-hydroxyquinoline (7HQ) [Tanner, C.; et al. *Science* **2003**, *302*, 1736]. Here, we study the analogous three-membered solvent-wire clusters $7HQ\cdot(NH_3)_n\cdot(H_2O)_m$, $n + m = 3$, using resonant two-photon ionization (R2PI) and UV−UV hole-burning spectroscopies. Substitution of H_2O for NH_3 has a dramatic effect on the excited-state H-atom transfer: The threshold for the ESHAT reaction is ~200 cm^{-1} for $7HQ\cdot(NH_3)_3$, ~350 cm^{-1} for both isomers of the $7HQ\cdot(NH_3)_2\cdot H_2O$ cluster, and ~600 cm^{-1} for $7HQ\cdot NH_3\cdot(H_2O)_2$ but increases to ~2000 cm^{-1} for the pure $7HQ\cdot(H_2O)_3$ water-wire cluster. To understand the effect of the chemical composition of the solvent wire on the H-atom transfer, the reaction profiles of the low-lying electronic excited states of the $n = 3$ pure and mixed solvent-wire clusters are calculated with the configuration interaction singles (CIS) method. For those solvent wires with an NH_3 molecule at the first position, injection of the H atom into the wire can occur by tunneling. However, further H-atom transfer is blocked by a high barrier at the first (and second) H_2O molecule along the solvent wire. H-atom transfer along the entire length of the solvent wire, leading to formation of the 7-ketoquinoline (7KQ*) tautomer, cannot occur for any of the H_2O-containing clusters, in agreement with experimentally observed absence of 7KQ* fluorescence.

1. Introduction

Modeling and understanding proton and hydrogen-atom transfer reactions are among the fundamental challenges in chemistry and biochemistry.[1−11] A topic of specific interest is proton transport through membrane channels ("proton wires"), because many transmembrane proteins create, control, or utilize proton gradients across biological membranes. Hydrogen-bonded wires of water molecules have been identified in membrane-spanning proteins such as bacteriorhodopsin,[12−15] photosystem II and bacterial photosynthetic reaction centers,[16−19] cytochrome oxidase,[20] and the transmembrane channel formed by gramicidin.[21−23] The enzymes carbonic anhydrase[24,25] and alcohol dehydrogenase[25] also contain proton relays along chains of water molecules embedded in the interior of the protein. The translocation mechanisms along these proton wires have become fields of intense theoretical study.[8,21−26] However, water wires do not per se result in efficient proton translocation; e.g., aquaporins allow water molecules to pass the membrane but selectively block the transfer of protons.[27−31] H-bonded ammonia wires have been detected in ammonia/ammonium transporter (Amt) transmembrane proteins, which are essential for nitrogen metabolism in all species.[32,33]

Direct experimental observation of H^+/H-atom transfer along water or ammonia wires would allow us to understand the factors controlling these processes. This is difficult in biological samples, because of the short times, heterogeneous environment and rapid solvent fluctuations involved. This complexity can be partially avoided by studying isolated and supersonically cooled model systems that also allow precisely controlled preparation of reactants and detection of products.[34−38]

Excited-state hydrogen-atom transfer reactions from organic chromophores to small solvent clusters have been studied intensively in recent years both spectroscopically and theoretically.[39−44] We employ the 7-hydroxyquinoline (7HQ) molecule as a molecular scaffold for the study of H-atom transfer along *mixed* hydrogen-bonded wires consisting of NH_3 and/or H_2O molecules. The solvent wire is connected by terminal H-bonds to the −OH and quinoline N groups, see Figure 1a. These induce a unidirectional hydrogen-bond pattern in the wire. Upon $S_1 \leftarrow S_0$ excitation the O−H group becomes more acidic and the quinoline N more basic. This drives an H-atom transfer reaction along the solvent wire, which is equivalent to a solvent-wire mediated enol → keto tautomerization reaction, resulting in excited-state 7-ketoquinoline (7KQ*) (cf. Figure 1b) with an inverted H-bond directionality. The $S_1 \rightarrow S_0$ fluorescence of 7KQ* is red-shifted relative to the enol UV fluorescence and can be employed to probe the proton/H-atom transfer reaction along the wire.[34−38]

Figure 1c shows a generalized reaction profile for excited-state H-atom transfer. As we will show, the relative energies of $\pi\pi^*$ excited enol (reactant) and keto (product) forms are rather insensitive to the chemical composition of the solvent wire. However, the $\pi\sigma^*$-state intermediate region of the profile in Figure 1c strongly depends on the identity of the solvent molecules: substitution of NH_3 by H_2O dramatically lowers the H-atom transfer rates. We first discuss the mass-specific $S_1 \leftarrow S_0$ resonant two-photon ionization spectra of the supersonically cooled mixed clusters $7HQ\cdot(NH_3)_n\cdot(H_2O)_m$ ($n + m = 3$) and the corresponding ammonia- and water-wire clusters $7HQ\cdot(NH_3)_3$ and $7HQ\cdot(H_2O)_3$. The latter have also been studied

* Corresponding author. E-mail: leutwyler@iac.unibe.ch.
† Present address: ETH Zürich, Lab. für Phys. Chemie, ETH-Hönggerberg, HCI, CH-8093 Zürich.

10.1021/jp056151b CCC: $33.50
Published on Web 01/10/2006

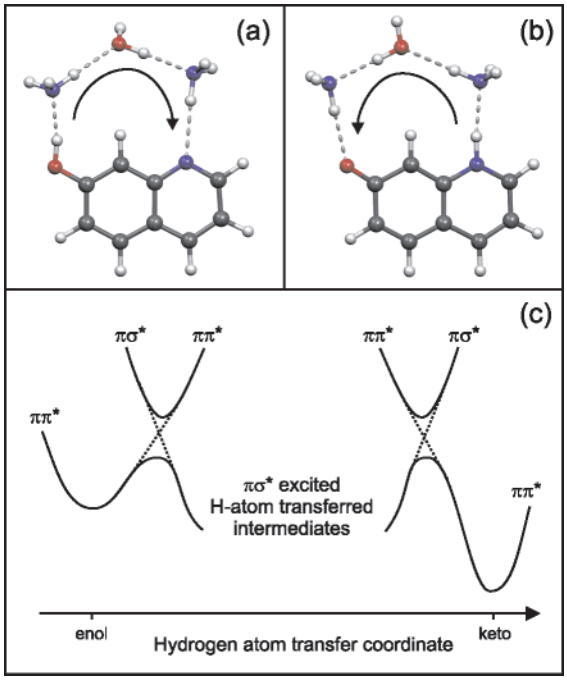

Figure 1. S_1-state optimized structures of the (a) enol and (b) keto tautomers of the 7-hydroxyquinoline·$(NH_3)_2$·H_2O cluster, *3ch3*-AWA. The arrows indicate the directionality of the hydrogen bonds, from donor to acceptor. (c) Generic excited-state hydrogen-atom transfer reaction profile for solvent-wire clusters attached to 7-hydroxyquinoline. Optical excitation occurs to the enol $\pi\pi^*$ state on the left.

previously.[34−38,45−48] Isomer-specific spectra are obtained by UV−UV hole-burning methods. The hydrogen-bond topologies and structures of the clusters are determined by comparing the spectra to electronic structure calculations. In the second part, we calculate and analyze excited-state H-atom transfer pathways for the different solvent-wire clusters and compare them to experiment.

2. Experimental Methods and Results

2.1. Experimental Methods. The 7HQ·$(NH_3)_n$·$(H_2O)_m$ clusters are synthesized and cooled in a 20 Hz pulsed supersonic expansion of Ne mixed with 0.5% NH_3. The carrier gas mixture at 1.5 bar passes through a tube containing ice cooled to ≈250 K (vapor pressure ∼0.8 mbar) and then into the magnetically actuated pulsed nozzle (0.5 mm diameter) containing 7-hydroxyquinoline (Spectrum), which is heated to ∼160 °C. Two-color resonant two-photon ionization (2C−R2PI) spectra are measured by crossing the jet with overlapping excitation and ionization laser beams inside the source of a linear time-of-flight mass spectrometer. $S_1 \leftarrow S_0$ excitation is performed with the frequency-doubled output of a Pyridine 1 dye laser at low pulse energies (50 μJ/pulse) to avoid optical saturation. All spectra are corrected for variations in laser power. The ionization laser (frequency-doubled Sulforhodamine B dye at 293 nm, ∼1 mJ/pulse) is spatially and temporally fully overlapped with the excitation laser. For UV−UV hole-burning spectroscopy a third laser pulse precedes the 2C−R2PI experiment by 100−300 ns. The burn laser frequency is fixed at an electronic origin or other strong band while scanning the 2C−R2PI excitation laser.[34−38]

2.2. Resonant Two-Photon Ionization and UV−UV Hole-Burning Spectra. Figure 2 shows the 2C−R2PI spectra of the 7HQ·$(NH_3)_n$·$(H_2O)_m$, $n + m = 3$ clusters starting from below the $S_1 \leftarrow S_0$ electronic origins. The spectra were measured 20−40 μs after the beginning of the gas pulse, to avoid any contributions from dissociation of larger clusters or cluster ions

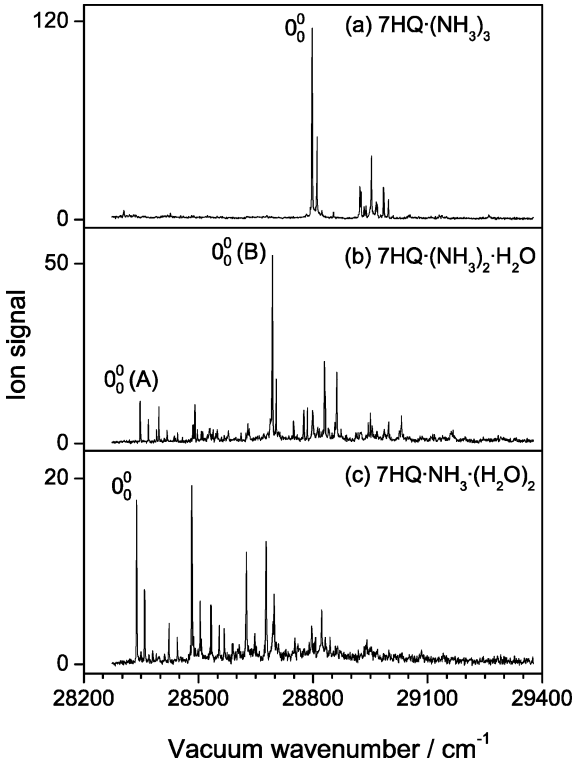

Figure 2. Two-color resonant two-photon ionization (2C−R2PI) spectra of the $S_1 \leftarrow S_0$ transitions of the 7-hydroxyquinoline·$(NH_3)_n$·$(H_2O)_m$, $n + m = 3$ clusters, recorded in the mass channels (a) 196 *u*, (b) 197 *u* and (c) 198 *u*. The ionization wavelength is 292.8 nm. The spectrum of 7-hydroxyquinoline·$(NH_3)_2$·H_2O in (b) is a superposition of two isomers, denoted A and B, cf. Figure 3c. The electronic origins are listed in Table 1.

TABLE 1: Electronic Origins of All Clusters 7HQ·$(NH_3)_n$·$(H_2O)_m$, $n + m = 3$ and Assigned Structures

cluster composition	electronic origin/cm^{-1}	assigned structure
7HQ·$(NH_3)_3$	28798	3*ch3*[a]
7HQ·$(NH_3)_2$·H_2O	28348	3*ch3*-AAW
7HQ·$(NH_3)_2$·H_2O	28694	3*ch3*-AWA
7HQ·NH_3·$(H_2O)_2$	28339	3*ch3*-AWW
7HQ·$(H_2O)_3$	28770	3*ch3*[b]

[a] Reference 37. [b] Reference 57.

into these mass channels. The 2C−R2PI spectrum of 7HQ·$(NH_3)_3$, Figure 2a displays an intense electronic origin at 28 798 cm^{-1} followed by ammonia-wire stretching vibrations up to 200 cm^{-1} above the origin. Above 200 cm^{-1} the R2PI spectrum falls off abruptly, and only traces of band structure are observed. Parallel to the loss of the R2PI signal, the UV fluorescence of the enol tautomer decreases whereas the yellow fluorescence of the keto tautomer increases.[34−38]

The spectrum of 7HQ·$(NH_3)_2$·H_2O in Figure 2b begins at 28 348 cm^{-1} with a group of weaker bands, followed by stronger bands starting at 28 694 cm^{-1}. UV−UV hole-burning measurements allow us to separate the spectral contributions of two isomers with electronic origins at 28 348 cm^{-1}, denoted isomer A, and 28 694 cm^{-1}, denoted isomer B. UV−UV hole-burning measurements of the 7HQ·NH_3·$(H_2O)_2$ cluster at the strong band at 28 339 cm^{-1} (see Figure 2c) results in a decrease of all the bands of the 2C−R2PI spectrum; hence there is only one isomer of this cluster. The electronic origins are given in Table 1 along with the structure assignments (see below).

In Figure 3, the electronic origins of these three $S_1 \leftarrow S_0$ spectra are aligned with those of the pure ammonia- and water-wire clusters. The spectra of isomers A and B of the 7HQ·

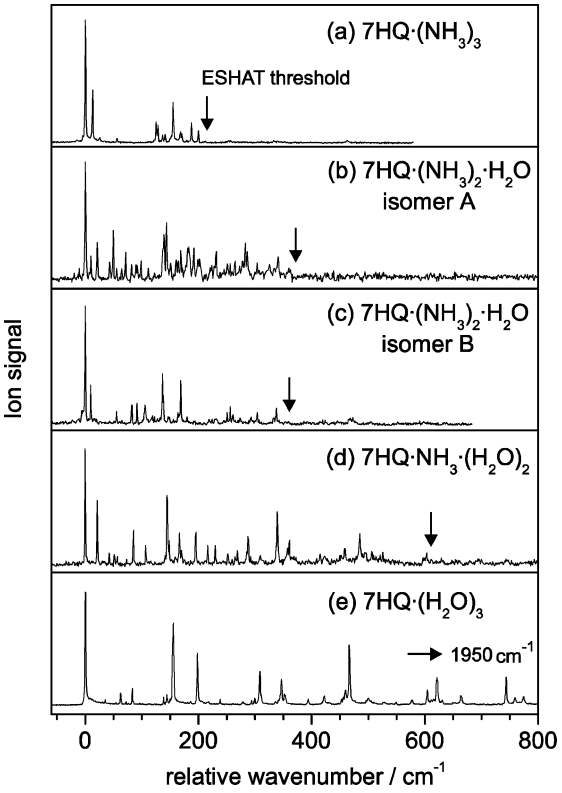

Figure 3. Isomer-selected $S_1 \leftarrow S_0$ absorption spectra of the 7HQ·$(NH_3)_n$·$(H_2O)_m$, $n + m = 3$ clusters. All spectra are plotted relative to their respective electronic origins. Traces (a), (d) and (e) are 2C−R2PI spectra, traces (b) and (c) are hole-burning difference spectra. The arrows indicate the breaking off of the vibrational level structure in the S_1 state.

$(NH_3)_2$·H_2O cluster have been separated by hole burning; cf. Figure 2b. The excess vibrational frequencies of the highest vibronic bands in the spectra, indicated by arrows in Figure 3, are clearly correlated with the number of H_2O molecules in the wire. For 7HQ·$(NH_3)_3$ the vibronic structure essentially vanishes ~200 cm^{-1} above the electronic origin. For both isomers A and B of 7HQ·$(NH_3)_2$·H_2O, the R2PI spectra break off at ≈350 cm^{-1} above their electronic origins. The $S_1 \leftarrow S_0$ spectrum of 7HQ·NH_3·$(H_2O)_2$ breaks off even higher, at ~600 cm^{-1}. Finally, the 7HQ·$(H_2O)_3$ cluster exhibits sharp vibronic bands up to 1950 cm^{-1}; the lower 900 cm^{-1} of the spectrum are shown in Figure 3.

In previous work,[34−38] we have shown that the breaking off of the R2PI spectrum of 7HQ·$(NH_3)_3$ is due to the onset of a fast H-atom transfer reaction in the S_1 excited state. Figure 3 shows that the mixed clusters with one or two NH_3 molecules replaced by H_2O exhibit a similar breaking off as the ammonia-wire cluster, but at increasingly higher excess vibrational energies. In contrast, the spectrum of the water-wire cluster extends to much higher excess energies. From these systematic shifts, we conclude that (a) The presence of at least one NH_3 molecule in the solvent wire can induce the excited-state reaction with an excess vibrational energy below 600 cm^{-1}. (b) The reaction threshold increases with the increasing number of water molecules within the wire. (c) The increase is highly nonlinear for $n = 1-3$ water molecules. (d) For the 7HQ·$(NH_3)_2$·H_2O-wire cluster, the reaction threshold does not seem to depend on the isomer.

The observation that the ESHAT reaction induces a rapid breaking off of the $S_1 \leftarrow S_0$ electronic spectrum implies (i) that the reaction product has a higher ionization potential, (ii) that the reaction product has a much lower ionization cross-section than the enol cluster, or (iii) that the HTn forms have additional fast deactivation channels such as intersystem crossing. Regarding (ii), we show in section IV that the ESHAT reaction products are diffuse Rydberg-type states that are spread over one or more molecules in the solvent-wire cluster. Because the ionization cross section of atomic and molecular Rydberg states are typically smaller than those of core-valence states,[49] the lower ionization cross sections can be a reason for the loss of ion signal. Regarding (iii), the singlet/triplet coupling may be especially efficient in the HT*n* forms due to the biradical nature of the $\pi\sigma^*$ state, in which the singlet and triplet potentials are nearly degenerate. We have recently discussed relaxation to 7HQ triplet states as a competitive mechanism to ESHAT for the 7HQ·$(NH_3)_3$ cluster.[38]

3. Theoretical Methods and Results

The 2C−R2PI spectra are now attributed to a specific cluster structure on the basis of electronic structure calculations for the ground and excited states. These methods have been applied successfully for the structural determination of the 7HQ·$(NH_3)_3$ cluster.[37] We then show how the excited-state reactivity is related to the number and sequence of NH_3 and H_2O molecules in the wire. All ab initio calculations were performed using Gaussian03.[50]

3.1. Calculated Structures and Binding Energies. The cluster geometries were optimized using DFT theory with the B3LYP functional[51] and the 6-311++G(d,p) basis set. Very stringent convergence criteria were applied: RMS difference $<10^{-9}$ between density matrix elements of consecutive SCF cycles, maximum component of the nuclear gradient $<2 \times 10^{-6}$ hartree/bohr or hartree/rad, and a pruned (99,590) grid for numerical integration. Normal-mode analyses were carried out for all optimized structures, yielding harmonic vibrational frequencies and zero-point vibrational energies (ZPVE). The binding energies D_e and dissociation energies D_0 (D_e corrected for ZPVE differences between the cluster and its constituent molecules) were calculated. Corrections for the basis set superposition error (BSSE) were applied with the full counterpoise method.[52]

For 7HQ·$(NH_3)_3$ there are three low-lying isomers with different binding topologies, denoted *3ch3* (chain of three solvent molecules between the functional groups), *3cy3* (cycle of three solvent molecules binding back to the O-atom lone pair) and *3ch2cy2* (chain of two solvent molecules and cycle of two solvent molecules with one solvent molecule joining both structures).[37,48] The *3ch3* isomer of 7HQ·$(NH_3)_3$ is the only isomer experimentally observed so far, but this does not carry over to the mixed clusters. To distinguish the sequence of solvent molecules, starting from the O−H group of 7HQ, we added a suffix (A for ammonia, W for water). All possible sequence permutations of the three forms *3ch3*, *3ch2cy2* and *3cy3* were calculated, i.e., nine isomers for 7HQ·$(NH_3)_2$·H_2O and 7HQ·NH_3·$(H_2O)_2$ each. The nine structures for 7HQ·$(NH_3)_2$·H_2O are shown in Figure 4. Note that for *3ch2cy2*−WAA the O−H···O−H···N−H···O cycle breaks open during the course of geometry optimization; see Figure 4. For 7HQ·NH_3·$(H_2O)_2$, we show only the three *3ch3* forms in Figure 5.

The calculated binding and dissociation energies D_e and D_0 of all eighteen clusters are given in Table 2. The *3ch3* isomers are clearly the most stable, with 2−3 kcal/mol larger binding energies than the most stable *3cy3* or *3ch2cy2* forms. On the basis of these results, we tentatively attribute the isomers A and B of 7HQ·$(NH_3)_2$·H_2O to the forms *3ch3*-AAW and *3ch3*-

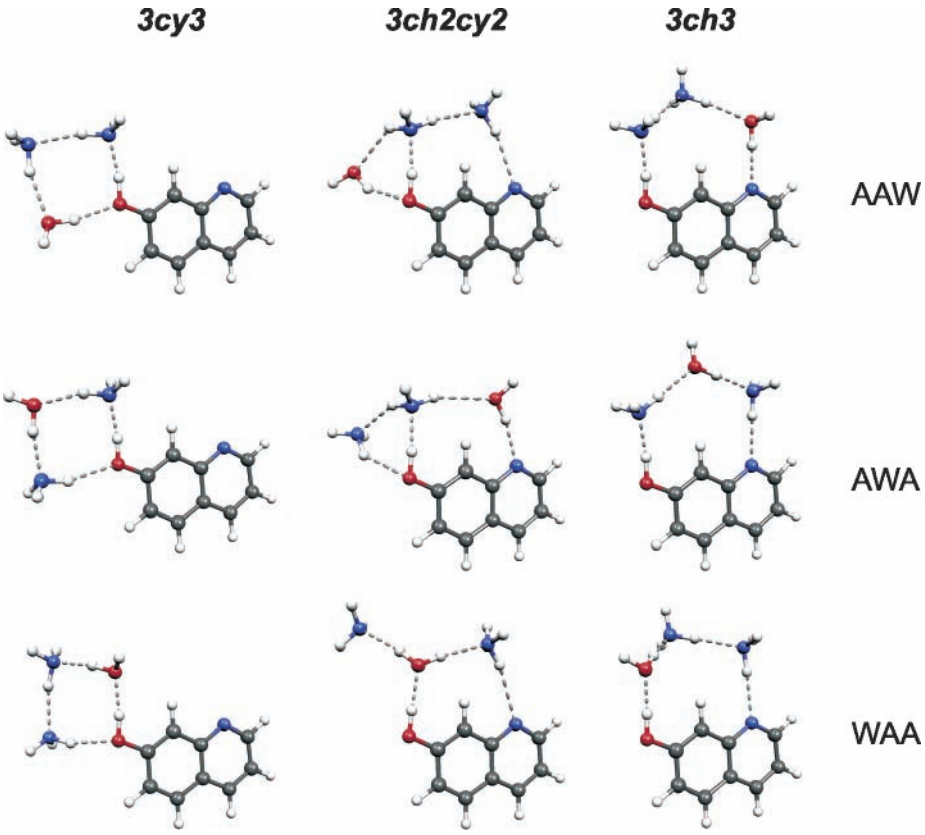

Figure 4. Nine B3LYP/6-311++G(d,p) minimum energy structures found for 7HQ·$(NH_3)_2$·H_2O. The clusters are grouped in columns according to their solvent topology and in rows according to the composition suffix.

AWA; see Figures 4 and 5. However, the small difference of 0.5 kcal/mol between the two forms does not warrant a definite assignment. The single observed isomer of 7HQ·NH_3·$(H_2O)_2$ is tentatively assigned to the *3ch3*-AWW isomer; however, the *3ch3*−WAW sequence is only 0.8 kcal/mol less stable. For several clusters, further isomers exist with a different local orientation of the "free" O−H bond of H_2O; these are not discussed here due to the small energy differences of <0.1 kcal/mol.

3.2. Calculated $S_1 \leftarrow S_0$ Electronic Transition Frequencies. These tentative isomer assignments are now tested by comparing the observed 0_0^0 frequencies to calculated transition frequencies. We employ time-dependent DFT with the same B3LYP functional and 6-311++G(d,p) basis set as for the structure optimizations. In Figure 6, we plot the TD-DFT vertical optical excitation energies frequencies vs the experimental 0_0^0 frequencies. The calculated/experimental values of bare 7HQ and the 7HQ·$(NH_3)_n$ and the 7HQ·$(H_2O)_n$ ($n = 1-3$) clusters are used as reference points, and these are connected by a parabolic least-squares fit in Figure 6. The different isomers of the mixed clusters can then be identified by comparing experiment and theory, as we have done previously for 7HQ·$(NH_3)_3$.[37]

Note that we compare *vertical* calculated excitations from ground-state optimized structures to *adiabatic* experimental excitations, the former being always higher. If we assume a contribution to excited-state relaxation due to the chromophore that is constant, the remaining difference between adiabatic and vertical transition energy is due to the response of the intermolecular coordinates to the geometric and electronic changes of the chromophore. This contribution is expected to increase for larger clusters, which justifies the use of a nonlinear reference curve.

In Figure 6 we plot the calculated TD-B3LYP excitations of the three different *3ch3* isomers. Because the 7HQ·$(NH_3)_2$·H_2O cluster has two origins, we plot the calculated origins twice in Figure 6a. The lower-frequency isomer A of 7HQ·$(NH_3)_2$·H_2O is clearly assignable as *3ch3*-AAW. On the other hand, isomer B gives a perfect match with the calculated *3ch3*-AWA isomer transition frequency. In Figure 6b for 7HQ·NH_3·$(H_2O)_2$, the calculated *3ch3*-AWW isomer electronic origin perfectly matches the experimental 0_0^0 frequency.

All three structure assignments based on the origin frequencies agree with the assignments based on the B3LYP ground-state binding energy calculations given in the previous section. Also, the relative stability of the two 7HQ·$(NH_3)_2$·H_2O clusters is correctly predicted by the B3LYP calculations: The more stable *3ch3*-AWA cluster (isomer B) gives rise to a spectrum that is approximately 5 times more intense than that of the *3ch3*-AAW isomer (isomer A); cf. Figure 2.

The $S_1 \leftarrow S_0$ excitation is fully localized on the 7HQ moiety; it should be sensitive to the proximal solvent molecules that form H bonds directly to 7HQ, and less susceptible to the molecule in the center of the wire. Figure 6 shows that the electronic origins of the clusters *3ch3*-AWW and *3ch3*-AAW, which differ only with respect to the central solvent molecule, agree within 9 cm^{-1}. The 7HQ·$(NH_3)_3$ and the *3ch3*-AWA cluster have the same contact solvent molecules and also have close-lying electronic origins; cf. Figure 6a.

4. Excited-State Hydrogen-Atom Transfer (ESHAT)

Having determined the H-bonding topologies, we now focus on the ESHAT reactions of the water-wire and mixed ammonia/water-wire clusters and investigate the influence of H_2O molecules in the wire on the excited-state H-atom transfer potentials, compared to the 7HQ·$(NH_3)_3$ ammonia wire that has been previously discussed.[34−38,47,48] The excited-state reaction

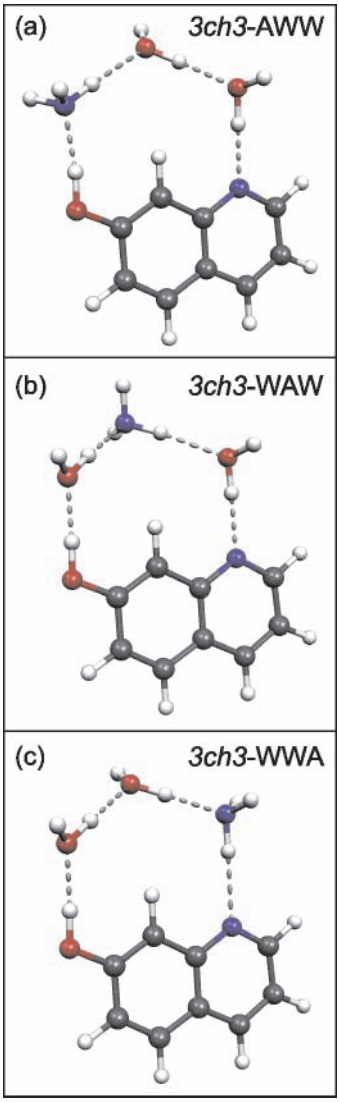

Figure 5. B3LYP/6-311++G(d,p) minimum energy structures found for the three chain forms of $7HQ{\cdot}NH_3{\cdot}(H_2O)_2$. A total of nine structures as in Figure 4 were calculated, cf. Table 2.

pathways are explored using the configuration interaction singles (CIS) method. The inclusion of very diffuse basis functions is crucial for the description of the Rydberg-type σ^* orbitals involved in the ESHAT reactions.[34,39,53,54] For the $7HQ{\cdot}(NH_3)_3$ cluster, the 6-31G(d,p) basis set was augmented with a set of diffuse s and p functions ($\alpha_s = 1.19 \times 10^{-2}$ bohr^{-1}, $\alpha_p = 3.74 \times 10^{-2}$ bohr^{-1}) on all H atoms involved in hydrogen bonds, abbreviated as 6-31(+)G(d,p).[34] To assess the effect of the diffuse functions on the stability of the mixed ammonia/water clusters, we also calculated the ESHAT profile of the $7HQ{\cdot}(H_2O)_3$ water wire with reoptimized diffuse exponents. These were $\alpha_s = 1.32 \times 10^{-2}$ bohr^{-1}, $\alpha_p = 3.49 \times 10^{-2}$ bohr^{-1}, very similar to those of the ammonia wire. Moreover, the energy differences between the stationary points calculated with the two different diffuse sets is ≤ 100 cm^{-1} for $7HQ{\cdot}(H_2O)_3$. For consistency, we use the previous basis set[34] for the calculations of mixed water/ammonia wires.

7-Hydroxyquinoline·$(H_2O)_3$. Figure 7 shows the CIS/6-31(+)G(d,p) calculated ESHAT potential of $7HQ{\cdot}(H_2O)_3$. Starting from the enol reactant minimum, the H atom is successively transferred to subsequent H_2O molecules in a series of Grotthus-type H-atom transfers. The transition state between the enol and HT1 forms is denoted $TS_{e/1}$ (and analogously for the other transition states. The intermediate minima are denoted HT1, HT2 and HT3. That this pathway corresponds to a hydrogen-atom transfer and *not* to a proton transfer is seen from the virtual orbitals that contribute dominantly to the S_1-state wave function, shown in Figure 7b. The relevant enol and keto orbitals are of π^* type and are delocalized over the aromatic 7-hydroxyquinoline framework. In contrast, the excited orbitals of the hydrogen-transferred forms HT1 to HT3 are diffuse Rydberg-type orbitals that extend over two water molecules. They are σ^* antibonding with respect to the O−H bonds.

The initial ESHAT steps occur by nonadiabatic coupling of the enol $\pi\pi^*$ excited state to a "dark" $\pi\sigma^*$ excited state. Stretching the O−H bond leads to a crossing of the $\pi\pi^*$ and

TABLE 2: Calculated Electronic Binding Energies (D_e), Changes in Zero Point Vibrational Energy (ΔZPVE), Binding Energies Corrected for ΔZPVE (D_0), Basis Set Superposition Error (BSSE) and BSSE Corrected Dissociation Energies (D_0^{CPC}) (All Values in kcal/mol)

		D_e	ΔZPVE	D_0	BSSE	D_0^{CPC}
		$7HQ{\cdot}(NH_3)_2{\cdot}H_2O$				
3cy3	AAW	−25.9	6.0	−19.9	2.6	−17.3
3cy3	AWA	−27.6	6.2	−21.4	2.6	−18.8
3cy3	WAA	−26.6	6.4	−20.2	2.9	−17.3
3ch2cy2	AAW	−24.0	6.0	−18.0	2.3	−15.7
3ch2cy2	AWA	−25.3	5.9	−19.4	2.2	−17.2
3ch2cy2	WAA	−27.0	6.4	−20.6	2.8	−17.8
3ch3	AAW	−29.5	6.4	−23.1	2.8	−20.3
3ch3	AWA	−29.9	6.3	−23.6	2.8	−20.8
3ch3	WAA	−28.5	6.4	−22.1	2.9	−19.2
		$7HQ{\cdot}NH_3{\cdot}(H_2O)_2$				
3cy3	AWW	−28.7	6.6	−22.1	2.9	−19.2
3cy3	WAW	−28.5	6.7	−21.8	3.2	−18.6
3cy3	WWA	−29.3	7.0	−22.3	3.2	−19.1
3ch2cy2	AWW	−26.3	6.2	−20.1	2.3	−17.8
3ch2cy2	WAW	−26.3	6.9	−19.4	2.8	−16.6
3ch2cy2	WWA	−28.5	6.8	−21.7	2.8	−18.9
3ch3	AWW	−33.4	6.9	−26.5	3.1	−23.4
3ch3	WAW	−32.6	6.9	−25.7	3.2	−22.5
3ch3	WWA	−32.1	7.0	−25.1	3.3	−21.8

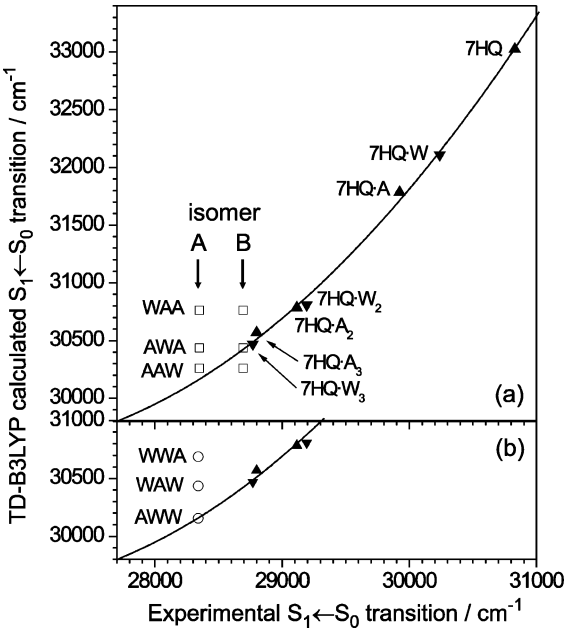

Figure 6. Calculated vertical TD-B3LYP $S_1 \leftarrow S_0$ transitions vs the experimental 0_0^0 transitions of the mixed ammonia/water-wire clusters. (a) Open squares: $7HQ{\cdot}(NH_3)_2{\cdot}H_2O$. (b) Open circles: $7HQ{\cdot}NH_3{\cdot}(H_2O)_2$ (b). The up triangles for $7HQ{\cdot}(NH_3)_n$, $n = 0-3$ and down triangles for $7HQ{\cdot}(H_2O)_n$, $n = 1-3$ are the points used for the fit.

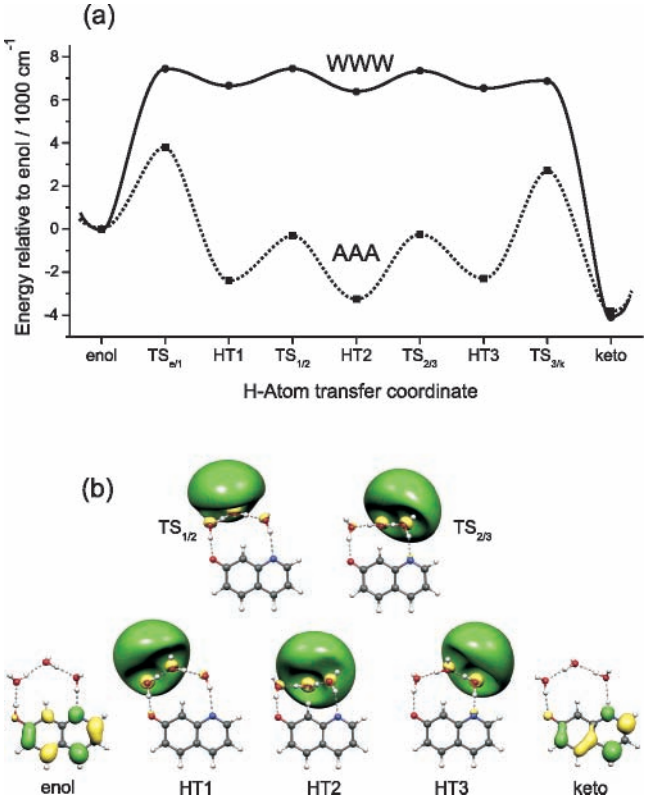

Figure 7. (a) CIS/6-31(+)G(d,p) calculated ESHAT profile for the 7HQ·$(H_2O)_3$ (WWW) and 7HQ·$(NH_3)_3$ (AAA) solvent-wire clusters. (b) Singly occupied virtual molecular orbitals that contribute dominantly to the S_1-state wave function for 7-hydroxyquinoline·$(H_2O)_3$ at the stationary points, with the exception of $TS_{e/1}$ and $TS_{3/k}$.

$\pi\sigma^*$ excited states, giving rise to a conical intersection. In an adiabatic description, the ESHAT reaction proceeds by tunneling through barrier regions that derive from the lower sheet of the conical intersection. This leads to formation of an H_3O (or NH_4 for the mixed and the pure ammonia wires) and 7-quinoxyl moiety coupled as a singlet biradical in the $\pi\sigma^*$ excited state. In the final ESHAT step a reverse $\pi\sigma^*/\pi\pi^*$-state crossing occurs upon N−H bond formation of the keto tautomer.

The ESHAT reaction profile of the water-wire cluster exhibits the same types of stationary points as 7HQ·$(NH_3)_3$, also shown in Figure 7a. However, the relative energies differ dramatically: For the ammonia wire the HT1-HT3 intermediates lie 2300−3250 cm^{-1} *below* the energy of the enol reactant, whereas for the water-wire cluster they all lie 6400−6800 cm^{-1} *above* the enol. For the water-wire cluster there is no driving force for the enol → HT1 nor for the subsequent HT1 → HT2 and HT2 → HT3 H-atom transfer steps. The barriers between subsequent HT*n* minima are ≈800 cm^{-1}, about 3 times smaller than for the ammonia wire. This is consistent with the observation that the diffuse σ^* orbital is delocalized over the H_3O and a neighboring H_2O molecule, whereas for the ammonia wire the corresponding orbitals are well localized on the NH_4 moieties. Interestingly, the overall enol → keto exoergicity is 300 cm^{-1} larger than for the ammonia wire.

7-Hydroxyquinoline·$(NH_3)_2$·H_2O. Figure 8 shows the ESHAT profile for the *3ch3*-AWA isomer, which corresponds to the experimentally observed isomer B. The ESHAT profile of 7HQ·$(NH_3)_3$ is again given for reference. The two reaction profiles are similar, except for the central part where NH_3 is replaced by H_2O. The initial H-atom transfer barrier $TS_{e/1}$ is 3970 cm^{-1} above the enol reactant, compared to 3790 cm^{-1} for the ammonia wire. The initial enol → HT1 step is

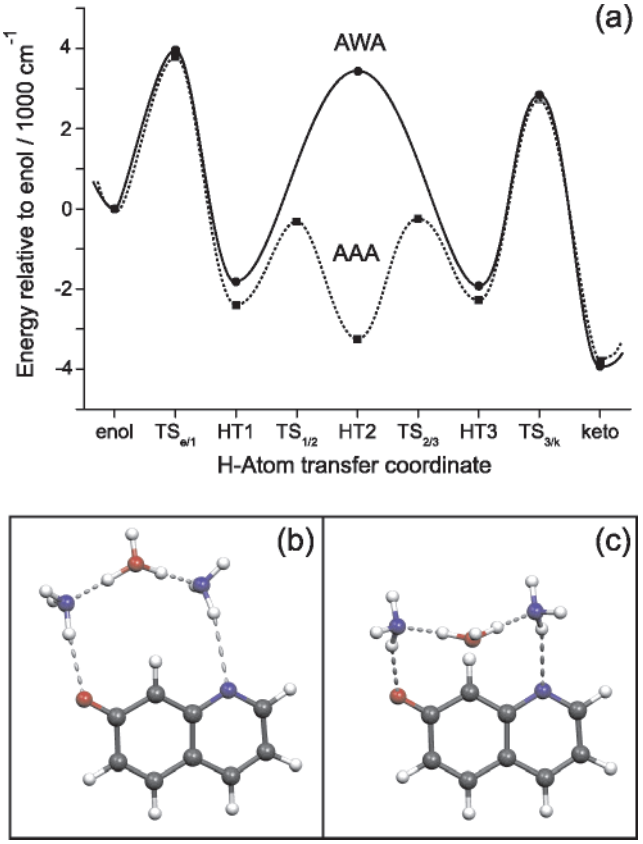

Figure 8. (a) CIS/6-31(+)G(d,p) ESHAT potential for the *3ch3*-AWA isomer. The 7HQ·$(NH_3)_3$ ESHAT potential is given as a reference (dotted line). Two different pathways for the HT1 → HT3 step were found: $HT2_{conc}$ (b) is a transition state, whereas HT2 (c) is a shallow minimum. HT2 lies 160 cm^{-1} above $HT2_{conc}$. The differences between the two pathways are too small to be shown on the energy scale of part (a).

less exoergic than for the ammonia wire (−1820 cm^{-1} compared to −2390 cm^{-1}). The CIS calculations predict two different HT1 → HT3 pathways: the first is a concerted transfer of two H atoms via the central H_2O, shown as the $HT2_{conc}$ form in Figure 8b. The corresponding ESHAT profile exhibits a saddle point 6690 cm^{-1} above the HT2 minimum of 7HQ·$(NH_3)_3$; cf. Figure 8a. The other pathway corresponds to a Grotthus-type H-atom transfer: the HT2 structure shown in Figure 8c is a shallow minimum. The transition structures $TS_{1/2}$ and $TS_{2/3}$ are structurally similar to the HT2 structure and lie only 6 cm^{-1} above HT2. Again, the overall enol → keto reaction is slightly more exoergic than for 7HQ·$(NH_3)_3$. The ESHAT profile of the *3ch3*-AAW isomer, shown in the collection of all ESHAT profiles (Figure 10), corresponds to a concerted reaction for the HT2 → keto step of the reaction. HT3 is a transition state 2460 cm^{-1} above the corresponding HT2 point of *3ch3*-AWA.

7-Hydroxyquinoline·NH_3·$(H_2O)_2$. The calculated ESHAT potential for the *3ch3*-AWW isomer is shown in Figure 9. The initial $TS_{e/1}$ barrier is 3960 cm^{-1}, 170 cm^{-1} higher than for the ammonia wire. The HT1 minimum lies 1390 cm^{-1} above that of 7HQ·$(NH_3)_3$. There are no stationary points corresponding to $TS_{1/2}$ and HT2; a steepest descent optimization starting from $TS_{2/3}$ leads directly to the HT1 structure. HT3 is a minimum energy structure but is 6250 cm^{-1} above the enol form. The last transition state ($TS_{3/k}$) lying 240 cm^{-1} above HT3 connects to the final keto product which is more than 10 000 cm^{-1} below. The overall enol → keto exoergicity is only 20 cm^{-1} smaller than for the ammonia wire.

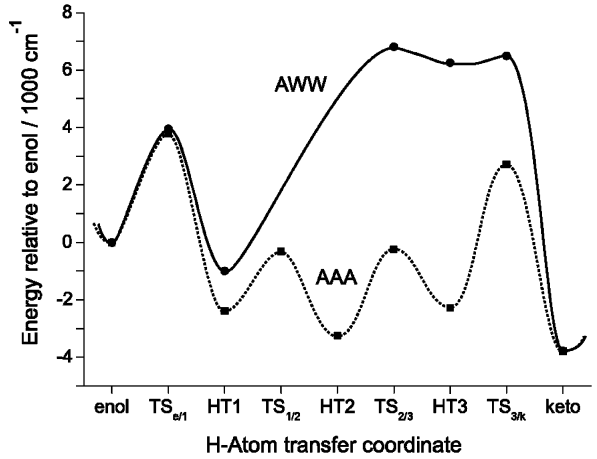

Figure 9. CIS/6-31(+)G(d,p) ESHAT potential of the *3ch3*-AWW cluster, cf. Figure 5a. The ESHAT potential of $7HQ\cdot(NH_3)_3$ is given as a reference.

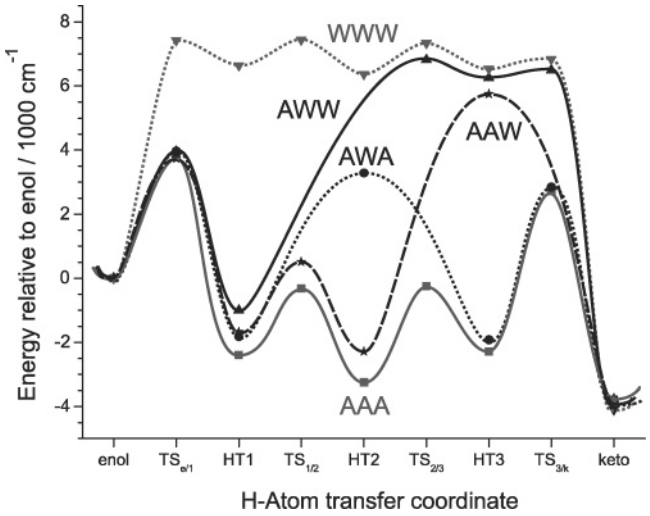

Figure 10. Overview of all ESHAT potentials from Figures 7−9. $7HQ\cdot(NH_3)_3$: solid gray. $7HQ\cdot(NH_3)_2\cdot H_2O$: dotted black (*3ch3*-AWA) and dashed black (*3ch3*-AAW). $7HQ\cdot NH_3\cdot(H_2O)_2$: solid black. $7HQ\cdot(H_2O)_3$: dotted gray.

5. Discussion

The ESHAT potentials discussed in the previous section are collected in Figure 10. For the $7HQ\cdot(NH_3)_3$ ammonia-wire cluster we have observed that the appearance of the 7KQ* keto fluorescence coincides with the disappearance of the enol R2PI spectrum.[34−38,47,48] For $7HQ\cdot(H_2O)_3$ there is no indication for any excited-state reactivity up to a vibrational energy of 1950 cm^{-1} nor has any keto fluorescence been observed so far.[45,46,55] This can be rationalized on the basis of the calculated ESHAT potentials: $TS_{e/1}$ and the HT1 forms for the water wire are significantly higher than for all the mixed clusters, and the first ESHAT reaction step is strongly endoergic (Figures 7 and 10).

For the mixed clusters, especially $7HQ\cdot NH_3\cdot(H_2O)_2$, the ESHAT pathway is also obstructed, rendering efficient enol → keto tautomerization impossible. Substitution of the central ammonia by H_2O leads to a perturbation of the ESHAT potential in the vicinity of HT2 and exchange of the last two ammonia molecules leads to a potential that closely follows that of the pure water-wire cluster between $TS_{2/3}$ and keto.

The ESHAT potentials of the AAA, AWA, AAW and AWW clusters have in common that (i) the enol → HT1 barriers are of similar height, (ii) the HT1 form is a minimum, and (iii) the enol → HT1 step is exoergic. This is paralleled by the experimental finding that the R2PI spectra of AWA, AAW and AWW all break off between 200 and 600 cm^{-1}, whereas there is no breaking off for the WWW pure water wire. Because the first step of the ESHAT reaction exhibits similar behavior for the $n = 3$ ammonia-wire and the three mixed clusters but differs from the pure water wire, the breaking off of the R2PI signal is clearly linked to the initial enol → HT1 step.

For $7HQ\cdot(NH_3)_3$, we have previously concluded from the large discrepancy between the calculated energy barrier and observed reaction threshold and from the marked isotope effect observed for the spectrum of the deuterated cluster that the initial $TS_{e/1}$ barrier is passed by tunneling.[34,37] We assume that tunneling also occurs for the mixed $7HQ\cdot(NH_3)_m\cdot(H_2O)_n$ clusters. However, it is very difficult to study the isotope effects for the mixed clusters: H/D substitution and NH_3/H_2O substitution both result in a mass difference of 1 *u*, so chemically different clusters have the same mass as isotopically different clusters.

The H-atom tunneling in the AAA, AWA, AAW and AWW clusters might be modeled with an effective one-dimensional treatment, as proposed by Cukier for excited-state proton transfer[7] in an asymmetric (metastable) potential well.[56] However, the H-atom enol → HT1 transfer involves not only motion of the H atom along the O−H···N hydrogen bond but also structural rearrangements within the solvent wire and the 7-hydroxyquinoline moiety. Thus, the tunneling rates depend not only on the barrier heights and curvatures[7] but also on the shape and length of the effective multidimensional tunneling reaction paths.

For the *3ch3*-AWW cluster the energy barrier between HT1 and keto is too high and wide to allow the formation of the keto tautomer. The situation is somewhat different for the *3ch3*-AWA wire, which is calculated to have an intermediate barrier comparable to $TS_{e/1}$ and $TS_{3/k}$. This barrier is, however, much wider in terms of *mass-weighted* coordinates than the $TS_{e/1}$ and $TS_{3/k}$ barriers: Not only do the two hydrogen atoms move in a concerted fashion, but also the whole H_3O moiety moves between the two ammonia molecules.

For $7HQ\cdot(NH_3)_3$ we have found that ≈40% of the clusters excited to the enol $\pi\pi^*$ state arrive at the keto $\pi\pi^*$ state; the remaining 60% are lost, probably by intersystem crossing to triplet states.[38] The reduced exoergicity of the initial ESHAT step for the mixed clusters might slow these deactivation kinetics and allow us to investigate the HT*n* forms, which would answer the question whether the breaking off of vibronic structure of the enol forms is due to a significantly higher ionization potential or a strongly reduced ionization cross section.

6. Conclusions

Resonant two-photon ionization and UV−UV hole-burning studies on the mixed ammonia/water solvent-wire clusters bound to 7-hydroxyquinoline show that the threshold for excited-state H-atom transfer increases with increasing number of H_2O molecules. The mass- and isomer-specific $S_1 \leftarrow S_0$ vibronic spectra of the different enol clusters break off at S_1-state excess energies ranging from 200 cm^{-1} for $7HQ\cdot(NH_3)_3$ to 600 cm^{-1} for $7HQ\cdot NH_3\cdot(H_2O)_2$. The breaking off of vibrational level structure is attributed to excited-state H-atom transfer (ESHAT), i.e., injection of the hydroxy group H atom into the solvent wire. Above a cluster-specific reaction threshold, the ESHAT rate becomes large enough to compete with the sum of the S_1-state radiative and other nonradiative processes. Raising the excess vibrational energy further leads to a steep increase of the ESHAT

rate, rapid depopulation of the enol S_1 state, and a breaking off of observable vibronic level structure. Substitution of all three NH_3 molecules by H_2O blocks the ESHAT reaction up to 1950 cm^{-1}.

Besides the pure ammonia- and water-wire clusters, two isomers of $7HQ{\cdot}(NH_3)_2{\cdot}H_2O$ and one isomer of $7HQ{\cdot}NH_3{\cdot}(H_2O)_2$ have been observed in the supersonic beam. The structural assignments of the latter three isomers are based (i) on B3LYP density functional calculations of the dissociation energies for 18 different cluster isomers and (ii) on calculations of the $S_1 \leftarrow S_0$ excitation frequencies using the time-dependent B3LYP method. Both methods confirm the hydrogen-bonded solvent-wire topology. The $7HQ{\cdot}(NH_3)_2{\cdot}H_2O$ isomers have the H-bond sequence ammonia−ammonia−water (AAW, isomer A) and ammonia−water−ammonia (AWA, isomer B). The H-bond sequence of $7HQ{\cdot}NH_3{\cdot}(H_2O)_2$ is ammonia−water−water (AWW).

CIS excited-state calculations of the ESHAT reaction profile show that partial substitution of NH_3 by H_2O molecules in the solvent wire allows the initial steps of the ESHAT reaction, i.e., one H-atom transfer in the clusters with the sequence AWA and ammonia−water−water AWW, or two successive H-atom transfers in the cluster AAW. In other words, the H-atom transfer is blocked by the first H_2O molecule along the wire. The AWA and AAW clusters both show an ESHAT threshold at ∼350 cm^{-1}, which implies that the first H-atom transfer gives rise to the observed threshold. The CIS calculations predict that the H-atom transfer along the entire wire should *not* occur for the AAW, AWA, AWW and WWW clusters, in agreement with the nonobservance of 7-ketoquinoline fluorescence from these clusters.

The initial ESHAT step is made possible by nonadiabatic coupling of the optically accessed enol $\pi\pi^*$ excited state to a dark $\pi\sigma^*$ excited state, giving rise to a conical intersection. The barrier heights for the enol → HT1 H-atom transfer reaction steps in the AAA, AAW, AWA, AWW clusters are related to the height of the respective conical intersections above the enol S_1-state minimum. The CIS calculations predict that the barrier height depends mainly on the proximal solvent molecule: for NH_3 it is ∼3500 cm^{-1} in the pure ammonia-wire cluster but increases by 150 cm^{-1} if one NH_3 molecule is replaced by H_2O and by 400 cm^{-1} if two NH_3 molecules are replaced by H_2O. For the $7HQ{\cdot}(H_2O)_3$ water-wire cluster the calculated barrier is 6500 cm^{-1} and the enol → HT1 H-atom transfer step is strongly endoergic, preventing the ESHAT reaction. The calculations are in qualitative agreement with the measured reaction thresholds of the ammonia/water clusters. Future calculations should include the effects of higher excitations and of dynamic correlation.

Acknowledgment. This work was supported by the Schweiz. Nationalfonds (project 200020-105490).

References and Notes

(1) Eigen, M.; Kruse, W.; Maass, G.; Maeyer, L. D. *Prog. React. Kinet.* **1964**, *2*, 285.
(2) Weller, A. *Prog. React. Kinet.* **1961**, *1*, 187.
(3) Agmon, N. *Chem. Phys. Lett.* **1995**, *244*, 456.
(4) Lu, D.; Voth, G. A. *J. Am. Chem. Soc.* **1998**, *120*, 4006.
(5) Vuilleumier, R.; Borgis, D. *J. Phys. Chem. B* **1998**, *102*, 4261.
(6) Cukier, R. I.; Nocera, D. G. *Annu. Rev. Phys. Chem.* **1998**, *49*, 337.
(7) Cukier, R. I.; Zhu, J. *J. Chem. Phys.* **1999**, *110*, 9587.
(8) Decornez, H.; Hammes-Schiffer, S. *Isr. J. Chem.* **1999**, *39*, 397.
(9) Hynes, J. T.; Tran-Thi, T.-H.; Granucci, G. *J. Photochem. Photobiol. A* **2002**, *154*, 3.
(10) Geissler, P. L.; Dellago, C.; Chandler, D.; Hutter, J.; Parrinello, M. *Science* **2001**, *291*, 2121.
(11) Tuckerman, M. E.; Marx, D.; Parrinello, M. *Nature* **2002**, *417*, 925.
(12) Stowell, M. H. B.; McPhillips, T. M.; Rees, D. C.; Soltis, S. M.; Abresch, E.; Feher, G. *Science* **1997**, *276*, 812.
(13) Sham, Y. Y.; Muegge, I.; Warshel, A. *Proteins: Structure, Function and Genetics* **1999**, *36*, 484.
(14) Subramaniam, S.; Henderson, R. *Nature* **2002**, *406*, 653.
(15) Garczarek, F.; Brown, L. S.; Lanyi, J. K.; Gerwert, K. *Proc. Natl. Acad. Sci.* **2005**, *102*, 3633.
(16) Baciou, L.; Michel, H. *Biochemistry* **1995**, *34*, 7967.
(17) Luecke, H.; Richter, H.-T.; Lanyi, J. K. *Science* **1998**, *280*, 1934.
(18) Tandori, J.; Sebban, P.; Michel, H.; Baciou, L. *Biochemistry* **1999**, *38*, 13179.
(19) Rémy, A.; Gerwert, K. *Nature Struct. Biol.* **2003**, *10*, 637.
(20) Michel, H. *Proc. Natl. Acad. Sci. U.S.A.* **1998**, *95*, 12819.
(21) Pomès, R.; Roux, B. *Biophys. J.* **2002**, *82*, 2304.
(22) Roux, B. *Acc. Chem. Res.* **2002**, *35*, 366.
(23) Pomès, R.; Yu, C.-H. *Front. Bioscience* **2003**, *8*, 1288.
(24) Jude, K. M.; Wright, K.; Tu, C.; Silverman, D. N.; Viola, R. E.; Christianson, D. W. *Biochemistry* **2002**, *41*, 2485.
(25) Cui, Q.; Karplus, M. *J. Phys. Chem. B* **2003**, *107*, 1071.
(26) Izvekov, S.; Voth, G. A. *J. Chem. Phys.* **2005**, *123*, 044505.
(27) Murata, K.; Mitsuoka, K.; Hirai, T.; Walz, T.; Agre, P.; Heymann, J. B.; Engel, A.; Fujiyoshi, Y. *Nature* **2000**, *407*, 599.
(28) de Groot, B. L.; Frigato, T.; Helms, V.; Grubmüller, H. *J. Mol. Biol.* **2003**, *333*, 279.
(29) Jensen, M. Ø.; Tajkhorshid, E.; Schulten, K. *Biophys. J.* **2003**, *85*, 1.
(30) Burykin, A.; Warshel, A. *Biophys. J.* **2003**, *85*, 3696.
(31) Ilan, B.; Tajkhorshid, E.; Schulten, K.; Voth, G. A. *Proteins − Struct., Funct. Bioinformat.* **2004**, *55*, 223.
(32) Khademi, S.; O'Connell, J.; Remis, J.; Robles-Colmenares, Y.; Miericke, L. J. W.; Stroud, R. M. *Science* **2004**, *305*, 1587.
(33) Zheng, L.; Kostrewa, D.; Berneche, S.; Winkler, F. K.; Li, X. D. *Proc. Natl. Acad. Sci. U.S.A.* **2004**, *101*, 17090.
(34) Tanner, C.; Manca, C.; Leutwyler, S. *Science* **2003**, *302*, 1736.
(35) Manca, C.; Tanner, C.; Leutwyler, S. *Chimia* **2004**, *58*, 287.
(36) Tanner, C.; Manca, C.; Leutwyler, S. *Chimia* **2004**, *58*, 234.
(37) Manca, C.; Tanner, C.; Coussan, S.; Bach, A.; Leutwyler, S. *J. Chem. Phys.* **2004**, *121*, 2578.
(38) Tanner, C.; Manca, C.; Leutwyler, S. *J. Chem. Phys.* **2005**, *122*, 204326.
(39) David, O.; Dedonder-Lardeux, C.; Jouvet, C. *Int. Rev. Phys. Chem.* **2002**, *21*, 499.
(40) Sobolewski, A. L.; Domcke, W.; Dedonder-Lardeux, C.; Jouvet, C. *Phys. Chem. Chem. Phys* **2002**, *4*, 1093.
(41) David, O.; Dedonder-Lardeux, C.; Jouvet, C.; Kang, H.; Martrenchard, S.; Ebata, T.; Sobolewski, A. L. *J. Chem. Phys.* **2004**, *120*, 10101.
(42) Lippert, H.; Stert, V.; Hesse, L.; Schulz, C. P.; Hertel, I. V.; Radloff, W. *Chem. Phys. Lett.* **2003**, *371*, 208.
(43) Lippert, H.; Stert, V.; Hesse, L.; Schulz, C. P.; Hertel, I. V.; Radloff, W. *Chem. Phys. Lett.* **2003**, *376*, 40.
(44) Lippert, H.; Stert, V.; Schulz, C. P.; Hertel, I. V.; Radloff, W. *Phys. Chem. Chem. Phys* **2004**, *6*, 2718.
(45) Bach, A.; Leutwyler, S. *Chem. Phys. Lett.* **1999**, *299*, 381.
(46) Bach, A.; Coussan, S.; Müller, A.; Leutwyler, S. *J. Chem. Phys.* **2000**, *112*, 1192.
(47) Bach, A.; Leutwyler, S. *J. Chem. Phys.* **2000**, *112*, 560.
(48) Coussan, S.; Meuwly, M.; Leutwyler, S. *J. Chem. Phys.* **2001**, *114*, 3524.
(49) Gallagher, T. F. *Rydberg Atoms;* Cambridge University Press: Cambridge, UK, 1994.
(50) Frisch, M. J.; Trucks, G. W.; Schlegel, H. B.; Scuseria, G. E.; Robb, M. A.; Cheeseman, J. R.; Montgomery, J. A., Jr.; Vreven, T.; Kudin, K. N.; Burant, J. C.; Millam, J. M.; Iyengar, S. S.; Tomasi, J.; Barone, V.; Mennucci, B.; Cossi, M.; Scalmani, G.; Rega, N.; Petersson, G. A.; Nakatsuji, H.; Hada, M.; Ehara, M.; Toyota, K.; Fukuda, R.; Hasegawa, J.; Ishida, M.; Nakajima, T.; Honda, Y.; Kitao, O.; Nakai, H.; Klene, M.; Li, X.; Knox, J. E.; Hratchian, H. P.; Cross, J. B.; Bakken, V.; Adamo, C.; Jaramillo, J.; Gomperts, R.; Stratmann, R. E.; Yazyev, O.; Austin, A. J.; Cammi, R.; Pomelli, C.; Ochterski, J. W.; Ayala, P. Y.; Morokuma, K.; Voth, G. A.; Salvador, P.; Dannenberg, J. J.; Zakrzewski, V. G.; Dapprich, S.; Daniels, A. D.; Strain, M. C.; Farkas, O.; Malick, D. K.; Rabuck, A. D.; Raghavachari, K.; Foresman, J. B.; Ortiz, J. V.; Cui, Q.; Baboul, A. G.; Clifford, S.; Cioslowski, J.; Stefanov, B. B.; Liu, G.; Liashenko, A.; Piskorz, P.; Komaromi, I.; Martin, R. L.; Fox, D. J.; Keith, T.; Al-Laham,

M. A.; Peng, C. Y.; Nanayakkara, A.; Challacombe, M.; Gill, P. M. W.; Johnson, B.; Chen, W.; Wong, M. W.; Gonzalez, C.; Pople, J. A. *GAUSSIAN 03*, revision A.1; Gaussian Inc.: Pittsburgh, 2003.
(51) Becke, A. D. *J. Chem. Phys.* **1993**, *98*, 1053.
(52) Boys, S. F.; Bernardi, F. *Mol. Phys.* **1970**, *19*, 553.
(53) Sobolewski, A. L.; Domcke, W. *Chem. Phys.* **2000**, *259*, 181.
(54) Sobolewski, A. L.; Domcke, W. *J. Phys. Chem. A* **2001**, *105*, 9275.
(55) Lahmani, F.; Douhal, A.; Breheret, E.; Zehnacker-Rentien, A. *Chem. Phys. Lett.* **1994**, *220*, 235.
(56) Miller, W. H. *J. Phys. Chem.* **1979**, *83*, 960.
(57) Bach, A.; Coussan, S.; Müller, A.; Leutwyler, S. *J. Chem. Phys.* **2000**, *113*, 9032.